Dynamical instabilities and *I-V* characteristics in resonant tunneling through double-barrier quantum well systems

Peiji Zhao and H. L. Cui
Department of Physics and Engineering Physics, Stevens Institute of Technology, Hoboken, New Jersey 07030

D. L. Woolard
Army Research Office, Research Triangle Park, North Carolina 27709

(Received 2 June 2000; published 18 January 2001)

Based on our time-dependent numerical simulation results of a resonant tunneling structure, a resonant tunneling theory for double-barrier quantum well systems (DBQWS's) is presented. The origin of intrinsic high-frequency current oscillation in DBQWS's, a long-time unsolved device physics problem, is explained, in terms of a time-dependent energy-level coupling model (TDELCM) as the result of the coupling between the emitter quantum well and the main quantum well and the wave-corpuscle duality of electrons. The origin of the intrinsic high-frequency current oscillation in DBQWS's and that of the hyteresis and plateaulike structure in *I-V* curves are two different aspects of the problem. A qualitative analysis of the creation of the hyteresis and plateaulike structure in *I-V* curves is also given. The TDELCM sets the foundation of the time-independent energy-level coupling model that was presented in our recent paper [P. Zhao *et al.*, J. Appl. Phys. **87**, 1337 (2000)]. It presents insight into the whole process of resonant tunneling through a DBQWS.

DOI: 10.1103/PhysRevB.63.075302 PACS number(s): 73.40.Gk, 72.20.−i

I. INTRODUCTION

The double-barrier resonant tunneling structure (DBRTS) has been extensively studied due to its novel physics and potential device applications. Until the late 1980s, resonant tunneling experimental results were qualitatively explained by the Chang-Esaki-Tsu (CET) theory.[1] At the end of the 1980s the experimental *I-V* characteristics of resonant tunneling through a double-barrier quantum-well system shows bistability and a plateaulike structure in the *I-V* curves.[2] The CET theory cannot explain the complicated experimental results. Historically, there is controversy regarding the explanation of the above-stated experimental result.

Since Goldman, Tsui, and Cunningham[2] (GTC) made the experimental discovery of the behavior of *I-V* characteristics of RTS's, it has attracted research attention for more than a decade.[3–17] There are three main theories explaining the experimental results. The first is the GTC theory.[2] In this theory, bistability is a nonlinear effect caused by electrostatic feedback experienced by the incoming electrons from the charge buildup in the space between the barriers. This view dominated the understanding of research in this area since this theory was presented. However, it has some serious drawbacks. As we know, charges build up in the well when the bias is applied on the devices. The amount of the charges in the well reach a maximum value just before the bias voltage reaches the resonance bias. Then, the charge density in the well decreases with the increase of the bias voltage. That is, the charge density in the well is higher when the bias voltage is close to the resonance bias. So, the electrostatic feedback should be stronger in vicinity of the resonance bias than that in the other bias region. Why does the plateaulike structure in the *I-V* curve exist at bias voltages away from the resonance bias voltage? Why is the plateaulike structure in the *I-V* curve created after the bias passes the resonance bias? The GTC theory cannot explain these problems. It also cannot explain why the plateaulike structure disappears at a certain bias voltage. The GTC theory can only predict the existence of two current states, but not the creation and disappearance of the plateaulike structure in the *I-V* curves. Thus, the GTC theory did not explain the origin of the hysteresis and plateaulike structure in the *I-V* curves. In fact, the GTC theory is based on the Schrödinger equation. A solution solely provided by solving the Schrödinger equation cannot give the plateaulike structure in *I-V* curve.[13] The second view on the origin of the hysteresis and plateaulike structure in the *I-V* curve of RTS's comes from Sollner.[11] Sollner believed that the bistability of the *I-V* curve occurred not because of the charging of the well, but because of the oscillation in the negative-resistance region. The oscillation in the negative-resistance region is caused by the external circuit. However, the research theory holding this point of view cannot explain all the features of the experimental results, for example, the plateaulike structure in the *I-V* curve.[14] Some people who support Sollner's view believe the bistability of *I-V* curve is extrinsic, caused by oscillation induced by an external circuit. However, numerical simulation results presented by Jensen and Buot,[4] Biegel and Plummer,[5] and Zhao and co-workers[16,17] clearly demonstrate that the oscillation and the bistability of *I-V* curve are intrinsic. Thus, Sollner's explanation is not a suitable answer to the problem; at the least it is incomplete. Jensen and Buot, the third research group, believed that the oscillation and the charging of the quantum well jointly contribute to the *I-V* characteristics of the RTS's which show hysteresis and a plateaulike structure in the curve.[4] Unfortunately, they did not provide a mechanism for the creation of the current oscillation.

Stated above are the main theories explaining the origin of the features of the experimental *I-V* curves. Although there are some researchers devoting to research in this

area,[6,10] their theories can be sorted into the above-mentioned three categories.

It should be noted that all theories cannot present a complete and self-consistent explanation of the experimental results. We believe that a suitable explanation of the experimental results should suitably and self-consistently explain the following issues: all features of the experiment, that is, two hystereses, a plateaulike structure in I-V curve. Also, why does the plateaulike structure in the I-V curve occur just after the current passes its main maximum value? Why does the plateaulike structure in the I-V curve start its formation while the charge density in the well is decreasing? Why does the plateaulike structure in the I-V curve disappear and at which bias point does it disappear? How do the hysteresis and plateaulike structure form? What factors determine the average slope of the plateaulike structure? The above-stated theories cannot answer all the questions. A complete and self-consistent explanation of the experimental results remained unknown for more than 10 years. Recently, the authors of this paper and Buot and Jensen presented an alternative understanding to the experimental results.[16] We noted the importance of the creation of an emitter quantum well just after the bias voltage passes the resonance bias.[18] The coupling between the energy level in the emitter quantum well (EQW) and that in the main quantum well (MQW) contributes to the creation of the plateaulike structure in the I-V curves. The coupling between the energy level in the EQW and the energy-band edge and the three-dimensional continuum states are the causes of the hysteresis. Our explanation of the experimental results are based on the stationary numerical simulation of the RTS's and a time-independent energy-level coupling model. With the energy-level coupling model, our theory can fully and self-consistently provide answers to the above-stated questions.

A problem closely related to the explanation of the hysteresis and plateaulike structure in the I-V characteristics curve of resonant tunneling through a double-barrier quantum well system is the origin of the intrinsic high-frequency current oscillation (IHFCO) in resonant tunneling. As stated above, Jensen and Buot observed the current instabilities in their numerical experiment on resonant tunneling. However, they did not present a complete and self-consistent explanation for the origin of the high-frequency current oscillation.[4] Historically, Ricco and Azbel first suggested, in their qualitative arguments, that intrinsic oscillation exists in a double-barrier structure for one-dimensional case.[19] They believed when the energy of the incoming electrons matches the resonance energy, the electrons enter the device and charge the potential well, raising the bottom, thus driving the system away from resonance. The ensuing current decrease lowers the charge in the well, bringing the system back to resonance, and a new cycle in the oscillatory behavior begins. The theory in Ref. 19 implies that the oscillation will occur at the resonance bias voltage. Numerical simulation results show that the bias voltages at which the current oscillates are different from the resonance bias voltage.[4,5,17] Presilla *et al.* believed that the nonlinearlity caused by the electrostatic feedback induced by the charge trapped in the well can lead to oscillation of the transmitted fluxes.[20] As we will explain later, electrostatic feedback is not the fundamental cause of the oscillation. Recently, Woolard *et al.* suggested that the current oscillation may be caused by the charge fluctuation near the emitter barrier of RTS's.[12] However, they did not present the cause of the charge oscillation near the emitter barrier and how the charge oscillation affects the electronic resonant tunneling. Obviously, a suitable theory accounting for this problem is still missing. A theory for explaining this problem should answer the following questions: How is the intrinsic high-frequency current oscillation created? Why does the time average of the time-evolving current give the plateaulike structure of the I-V curve? Why do the high-frequency oscillations exist only in a certain bias-voltage region? It should also be able to predict oscillation frequency.

In this paper, by numerically solving the coupled Wigner-Poisson equations, based upon our numerical calculation results, we present a TDELCM for explaining the origin of the IHFCO in resonant tunneling through double-barrier quantum well systems. In terms of this model, the above-mentioned two long-time unsolved problems, the origin of the hysteresis and plateaulike structure in the I-V characteristics of resonant tunneling and the origin of the high-frequency current oscillation in resonant tunneling, can be complete and self-consistently solved as a whole. In our theory, these two problems are different aspects of one problem: How do electrons pass a DBQWS? A clear picture of resonant tunneling through double-barrier quantum well systems can be obtained. This qualitative resonant tunneling theory presents new insights to resonant tunneling through a DBQWS.

This paper is organized as follows. In Sec. II, we briefly describe the numerical technique used in this paper. The numerical results, the time-dependent energy-level coupling model, and the explanation of the results are presented in Sec. III. The conclusion of this paper is given in Sec. IV of this paper.

II. NUMERICAL TECHNIQUE

The Wigner function formulation of quantum mechanics has been used in our approach, due to its many useful characteristics for the simulation of quantum-effect electronic devices, including the natural ability to handle dissipated and open-boundary systems. The Wigner function equation was first employed in quantum device simulation by Frensley.[3] Then, Kluksdahl *et al.* included the Poisson equation (PE) to the model of RTD and self-consistently solved this model.[6] The Wigner function equation (WFE) can be derived in several ways.[21] Since the Wigner function may be defined by nonequilibrium Green's functions, the WFE may be derived from the equation of motion of the nonequilibrium Green's function.[22,23] With only the lowest-order approximation to scattering being considered, we have

$$\frac{\partial f}{\partial t} = -\frac{hk}{2\pi m^*}\frac{\partial f}{\partial x} - \frac{1}{h}\int dk' f(x,k') \int dy [U(x+y) - U(x-y)] \sin[2y(k-k')] + \left.\frac{\partial f}{\partial t}\right|_{\text{coll}}, \tag{1}$$

where h is Planck's constant, m^* is the electron effective mass, and U is the conduction-band edge. Appropriately treating scattering in semiconductors is very important for getting necessary simulation results. Recent research shows that the computation burden associated with detailed consideration of electron-phonon scattering is formidable. Typical computer CPU times required for the calculation of one point in the *I-V* curve are the order of 30 h on a 100 CPU Cray T3E machine.[24] The huge amount of computation times would make this paper impossible if we treated the scattering in detail. Thus, we employed the relaxation-time approximation to scattering in this paper. In terms of the relaxation-time approximation to scattering, the collision terms in the above equation may be written as[22]

$$\left.\frac{\partial f}{\partial t}\right|_{\text{coll}} = \frac{1}{\tau}\left[\frac{f_0(x,k)}{\int dk\, f_0(x,k)}\int dk\, f(x,k) - f(x,k)\right], \tag{2}$$

where τ is the relaxation time and f_0 is the equilibrium Wigner function. The boundary conditions are

$$f_{x=0,k>0} = \frac{4\pi m^* k_B T}{h^2}\ln\left\{1+\exp\left[-\frac{1}{k_B T}\left(\frac{h^2k^2}{8\pi^2 m^*}-\mu_0\right)\right]\right\}, \tag{3}$$

$$f_{x=L,k<0} = \frac{4\pi m^* k_B T}{h^2}\ln\left\{1+\exp\left[-\frac{1}{k_B T}\left(\frac{h^2k^2}{8\pi^2 m^*}-\mu_L\right)\right]\right\}. \tag{4}$$

The second equation composing our RTD model is the Poisson equation (PE)

$$\frac{d^2}{dx^2}u(x) = \frac{q^2}{\epsilon}[N_d(x)-n(x)], \tag{5}$$

where ϵ is the dielectric permittivity, $u(x)$ is the electrostatic potential, q is the electronic charge, $N_d(x)$ is the concentration of ionized dopants, and $n(x)$ is the density of electrons, given by

$$n(x) = \int_{-\infty}^{\infty}\frac{dk}{2\pi}f(x,k). \tag{6}$$

The current density may be written as

$$j(x) = \int_{-\infty}^{+\infty}\frac{dk}{2\pi}\frac{\hbar k}{m^*}f(x,k). \tag{7}$$

To solve the WFE-PE equations, we must discretize the simulation zone and these two equations. For the one-dimensional device model, the discretization of the PE is trivial. We just present the discretization of the WFE. Details of this process are well described by Jensen and Buot.[4] So, only a summary of the results is given here. Assuming the simulation zone is between $x=0$ and $x=L$, the zone may be discretized as follows:

$$f(x,k) = f(x_i,k_j) = f_{ij}, \tag{8}$$

$$x_i = (i-1)L/(N_x-1) = (i-1)\,\delta x, \quad \delta x = L/N_x \tag{9}$$

$$k_j = (2j-N-1)\,\delta k/2, \quad \delta k = \pi/N\,\delta x, \tag{10}$$

where N_x and N are the number of x and k points on a grid in phase space. The time-dependent Wigner function equation can be written as

$$\frac{\partial f}{\partial t} = \frac{\mathcal{L}}{i\hbar}f, \tag{11}$$

where

$$\mathcal{L} = i(T+V+S). \tag{12}$$

In the above equation, T, V, and S are the drift, potential, and scattering terms, respectively. Using a second-order upwind difference scheme to discretize the position derivative, they can be expressed as

$$Tf(x,K) = -\frac{\hbar^2\delta k}{2m^*\delta x}(2j-N\text{-}1)\Delta^{\pm}f(i,j), \tag{13}$$

$$\Delta^{\pm}f(i,j) = \pm\tfrac{1}{2}[-3f(i)+4f(i\pm1)-f(i\pm2)], \tag{14}$$

$$Vf = \sum_{j'=1}^{N} V(i,j-j')f(i,j), \tag{15}$$

$$V(i,j) = \frac{2}{N}\sum_{i'=1}^{N/2}\sin\left[\frac{2\pi}{N}i'j\right][U(i+i')-U(i-i')], \tag{16}$$

and

$$Sf = \frac{\hbar}{\tau}\left\{f(i,j) - \frac{\delta k f_0(i,j)}{2\pi\rho(i)}\sum_{j'=1}^{N}f(i,j')\right\}. \tag{17}$$

The discretized density of electrons and current density may be written, respectively, as

$$n(i) = \frac{\delta k}{2\pi}\sum_{j=1}^{N}f(i,j) \tag{18}$$

and

$$J(i+\tfrac{1}{2}) = \frac{\hbar\,\delta k}{8\pi^2 m^*}\sum_{j=1}^{N}k_j \times\begin{cases}3f(i+1,j)-f(i+2,j), & j\leqslant\frac{1}{2}N\\ 3f(i,j)-f(i-1,j), & j>\frac{1}{2}N.\end{cases} \tag{19}$$

The formal solution of Eq. (11) is

$$f(t+\Delta t) = e^{-(i\mathcal{L}/h)t}f(t) = \frac{1-(i\mathcal{L}/2\hbar)t}{1+(i\mathcal{L}/2\hbar)t}. \tag{20}$$

This equation may be written as

$$[-r+\mathcal{L}][f(t+\Delta t)+f(t)] = -2rf(t), \tag{21}$$

where $r=2\hbar/\Delta t$. In discretizing the equation above, the drift term gives the boundary condition. The boundary condition does not change with time. Thus, we have

$$[-r+\tilde{\mathcal{L}}][f(t+\Delta t)+f(t)]=-2rf(t)+2\mathrm{BC}, \quad (22)$$

where $\tilde{\mathcal{L}}$ is the operator defined by Eq. (20) without considering the boundary conditions of Wigner function, that is, BC. In the discretization of Eqs. (1) and (5), the dielectric function of the material and the effective mass of electrons is taken to be constant throughout the structure.

In our simulation, we first approximate the conduction-band profile by a square well potential and get $n(x)$ from Eqs. (1) and (6). The density of electrons is substituted into the Poisson equation and then the new conduction-band profile $U(z)=u(z)+\Delta_c(z)$ is obtained, where $\Delta_c(z)$ is the offset of the band edge. Using this new conduction-band profile at the next time step, the Wigner function equation is solved again. This iteration continues until a steady-state or a preassigned time value is achieved by a simultaneous solution of both Eqs. (1) and (5).

In order to ensure the convergence of the numerical simulation results, we have employed a very small time step in our simulation. The time step is 1 fs. Furthermore, we have tested several structures with different momentum and position space mesh points and different simulation boxes to ensure correct simulation results. These results will be presented elsewhere. It should be noted that the numerical technique adapted in this paper is well established, having been used by many others previously with well accepted results. The correctness of the similar simulation results has been verified before.[3,4]

III. NUMERICAL RESULTS AND ANALYSIS

The intrinsic oscillation was first numerically observed by Jensen and Buot. Then, Biegel and Plummer got similar results. In order to compare our results to theirs, we consider the RTS extensively studied in the literature.[4,5] The parameters used in our simulation are the following. The momentum and position spaces are broken into 72 and 86 points, respectively. The donor density is 2×10^{18} particles/cm^3; the compensation ratio for scattering calculations is 0.3; the barrier and well widths are 30 and 50 Å, respectively; the simulation box is 550 Å; the barrier potential is 0.3 eV, corresponding to $Al_{0.3}Ga_{0.7}As$; the device temperature is 77 K except as noted otherwise; the effective mass of the electron is assumed to be a constant and equals $0.0667m_0$; the doping extends to 30 Å before the emitter barrier and after the collector barrier; the quantum well region is undoped. Bulk GaAs parameters are used to calculate the relaxation time and the chemical potential. The chemical potential is determined by $\int_0^\infty \sqrt{\epsilon} f(\epsilon) d\epsilon = \frac{2}{3}\mu(T=0)^{3/2}$, where $f(\epsilon)$ is the Fermi distribution function. This RTS is called RTS1 hereafter. The method of evaluating the relaxation time can be founded in Ref. 22.

A. Numerical results

Figure 1 shows the I-V characteristics of the resonant tunneling when the time-dependent simulation reaches steady state. In the current oscillation region, the current values are determined by averaging over a period. This figure shows all the features of the experimental results: a plateau-like structure in the I-V characteristics and two hystereses regions. It convinces us of the correctness of our numerical calculation.

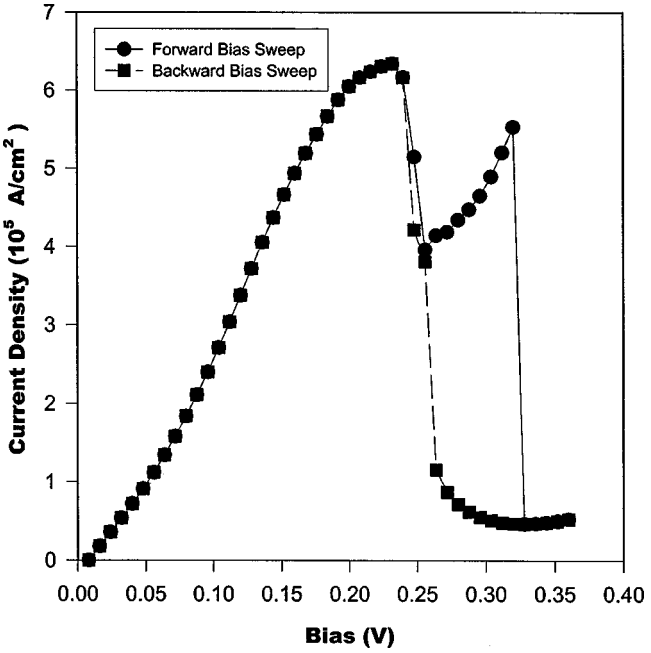

FIG. 1. I-V characteristics of the RTD. The data are taken from the steady states of the simulation. The values of the current in the BVW are calculated from time average of the current oscillation.

Figure 2 shows the time-dependent current density with bias voltage as a parameter. This figure exhibits the following features of the time-dependent current density: The oscillation of current density starts after the bias voltage passes the resonance bias (0.224 V); there is a bias-voltage window (BVW) in which the current oscillation is permanent; the amplitude of the oscillated current is variable; as the bias voltage approaches the BVW from the low-bias-voltage side, the amplitude of the current density increases, and the opposite phenomena for the amplitude exists as the bias voltage goes away from the BVW on the high-bias-voltage side. The current oscillation in the BVW can last a very long period of time. In our simulation, we have chosen the simulation for the current oscillation in the bias-voltage window to be 30 ps at a bias voltage of 0.248 V. The frequency of the oscillation is the order of 1 THz. No obvious reduction of the amplitude of the current oscillation has been found.

In order to understand the cause the current oscillation, we plot the time-dependent self-consistent potential and electron density at different bias voltages. These graphs are presented in Figs. 3–10 for the case of forward bias sweep. From these figures we can see that the current oscillation is concurrent with those of potential and electron density in the whole region of the device. The oscillations have the following features. Before the bias reaches the BVW, the potential and electron density just irregularly oscillate a short time and then evolve into steady state. When the bias voltage enters

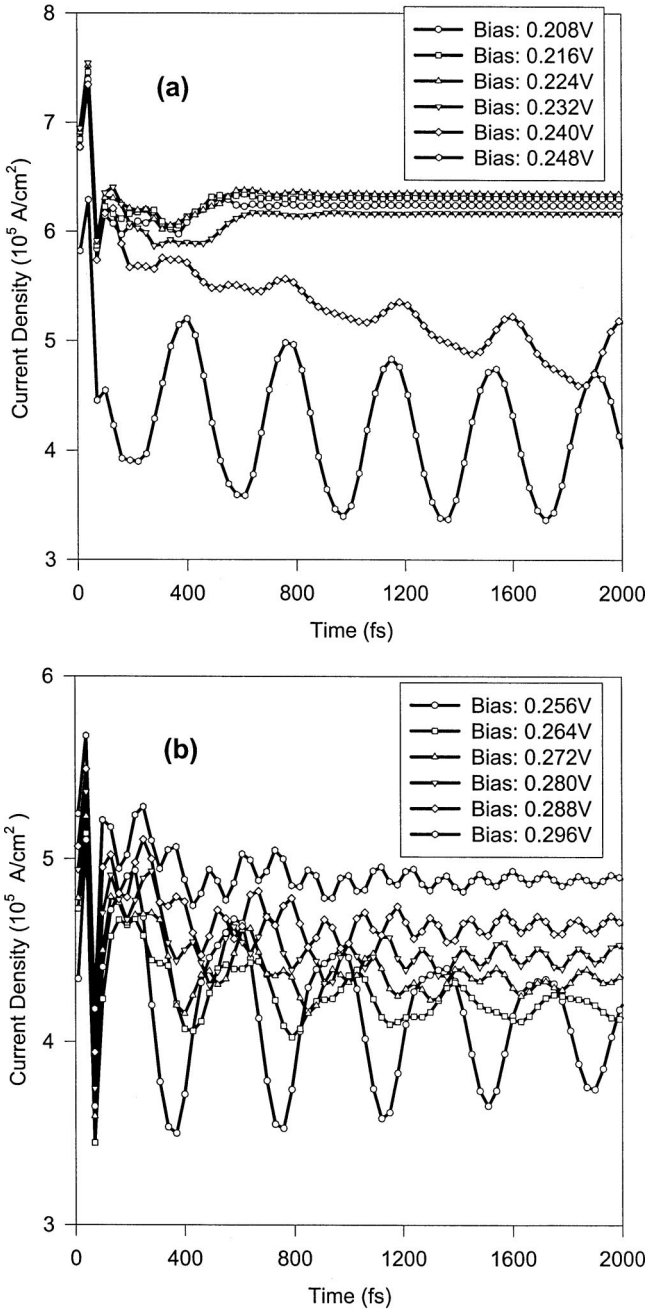

FIG. 2. Current-time characteristics of the RTD with bias voltages as parameters for the case of forward bias sweep.

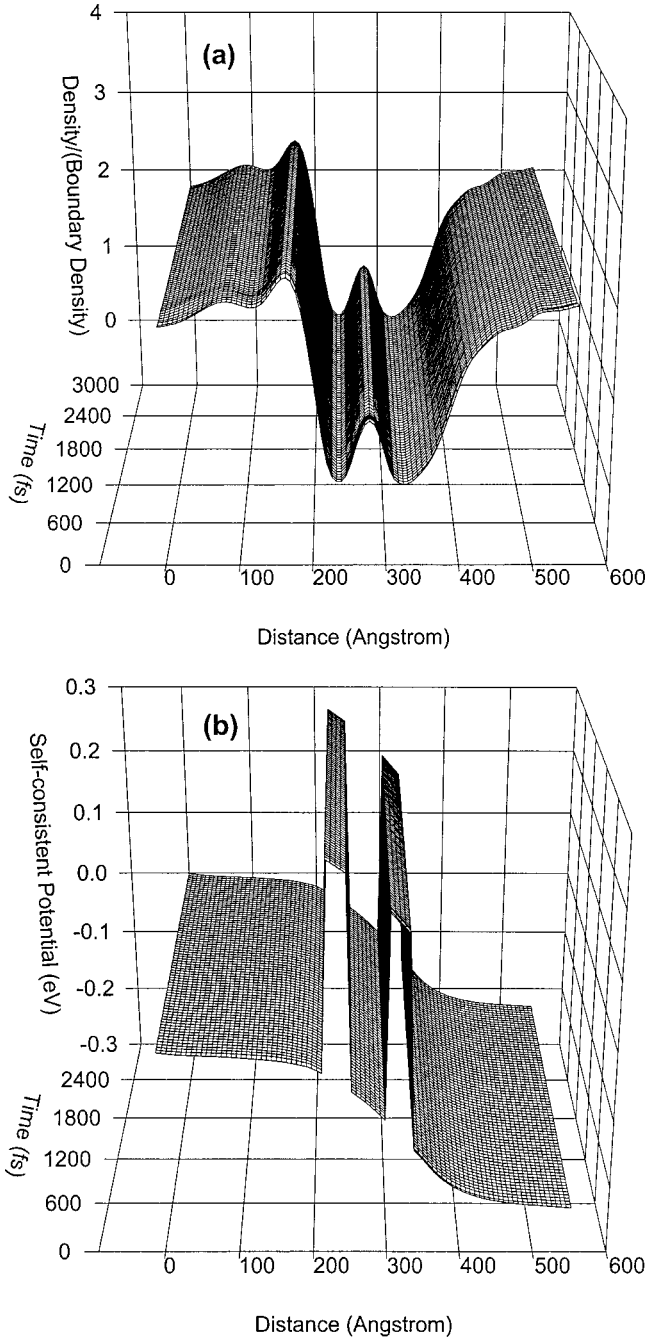

FIG. 3. Time-dependent electron density distribution, (a) self-consistent potential and (b) at bias voltage 0.232 V. The self-consistent potential shows that there is no an emitter quantum well in front of the emitter barrier. After a few irregular oscillations, the density distribution of electrons enters the steady state. The density in the MQW remains at a higher value.

the BVW, the potential and the electron density oscillate periodically rather than irregularly. The density oscillation is stronger than that of the potential. The density oscillation in front of the emitter barrier is stronger than that in the MQW. These features do not support the Ricco-Azbel theory on the origin of the instability in double-barrier systems. In the BVW, at a special bias voltage (0.248 V), the irregular oscillations of the potential and electron density last a very short time. The potential and electron density enter into stable oscillations almost directly without experiencing a damping state. After the bias voltage exists from the BVW in the higher-bias-voltage direction, if the bias voltage is high enough, the current oscillation becomes damped, as do the potential and electron density. This is true especially when current density is in the plateaulike structure of the *I-V* curve of RTD. This situation lasts until the bias voltage reaches a special point where the plateaulike structure in the *I-V* characteristics collapses.

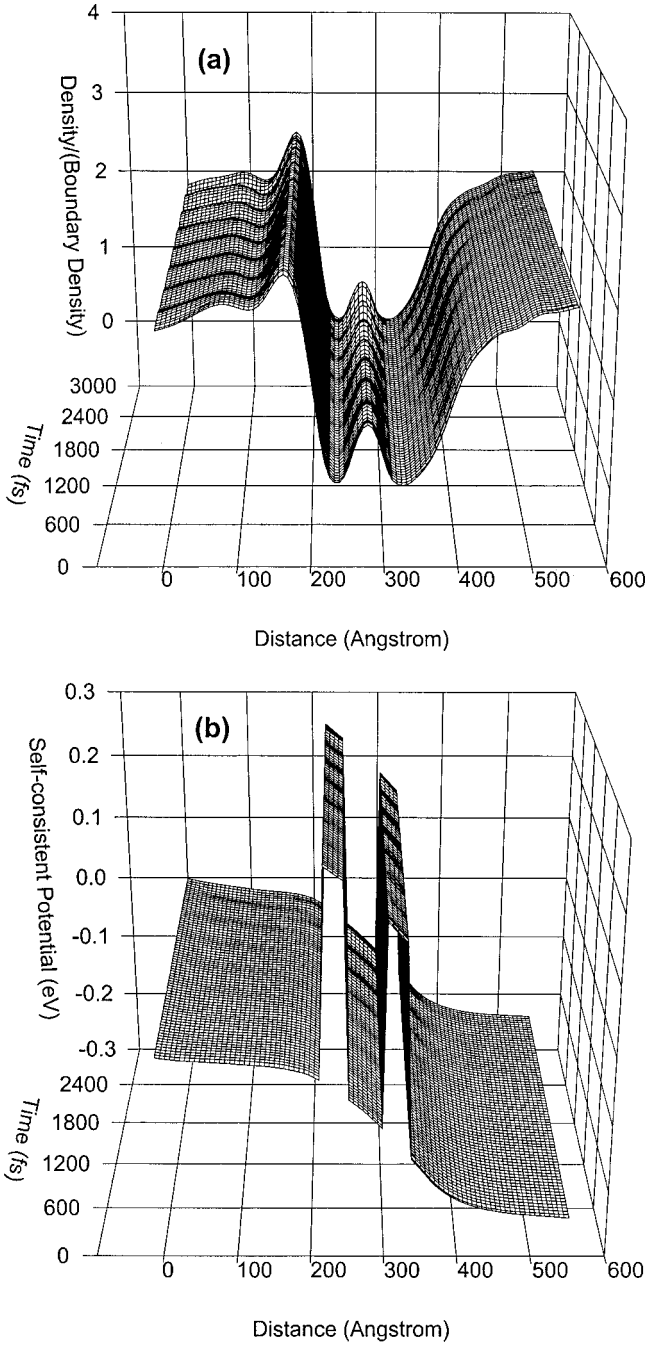

FIG. 4. Time-dependent electron density distribution, (a) self-consistent potential and (b) at bias voltage 0.240 V. The density distribution in the emitter shows a stronger oscillation than that in the MQW and the oscillation amplitude increases with the increase of simulation time. The self-consistent potential shows the creation process of an EQW and the development of the potential oscillation.

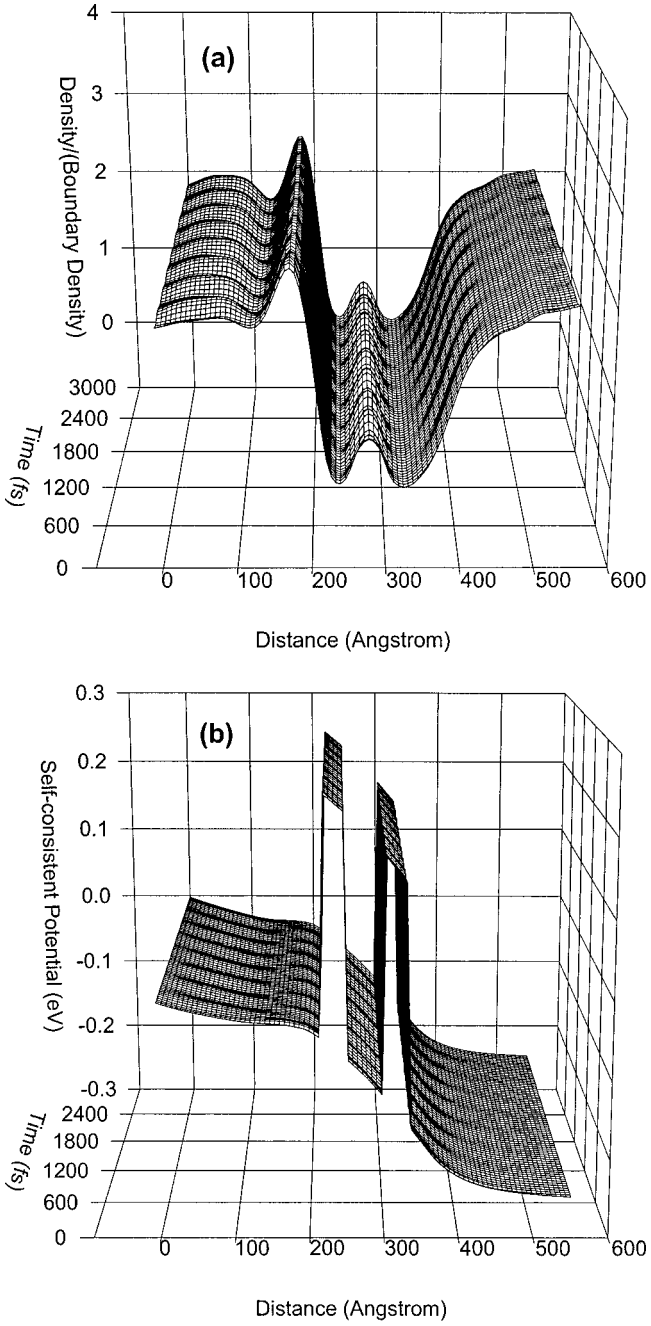

FIG. 5. Time-dependent electron density distribution, (a) self-consistent potential and (b) at bias voltage 0.248 V. The figures show the oscillation of potential and density distribution in stable states. It should be noted that the depth of the EQW is increasing.

Referring to Figs. 1 and 9, when the plateaulike structure in the I-V curve disappears, we can see that the EQW disappears with increasing simulation time. Subsequently, for different bias voltages, the evaluation of the current, potential, and electron density with respect to time is all the same before the second energy level in the MQW falls to the electron Fermi level in the emitter. The average of the time-dependent electron density distributions in the MQW decreases after the bias passes the resonance bias voltage. While the bias voltage stays in the plateaulike structure of I-V curve, the electron density in the MQW almost remains unchanged [see Figs. 5(a) to 7(a)]. Once the EQWdisappears, the electron density in the MQW reduces dramatically. Then, the density keeps at an unchanged, low value in the MQW.

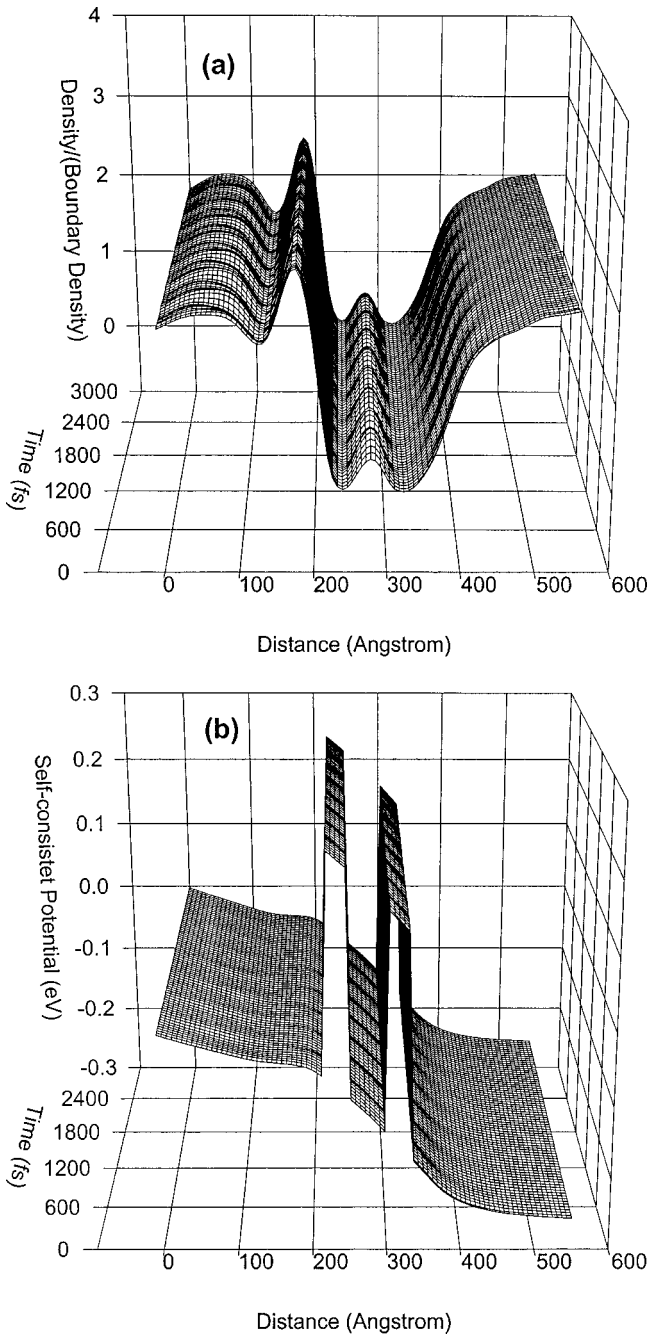

FIG. 6. Time-dependent electron density distribution, (a) self-consistent potential and (b) at bias voltage 0.256 V. The figures show the oscillation of potential and density distribution are becoming week with the increase of time. It should be noted that the depth of the EQW is increasing.

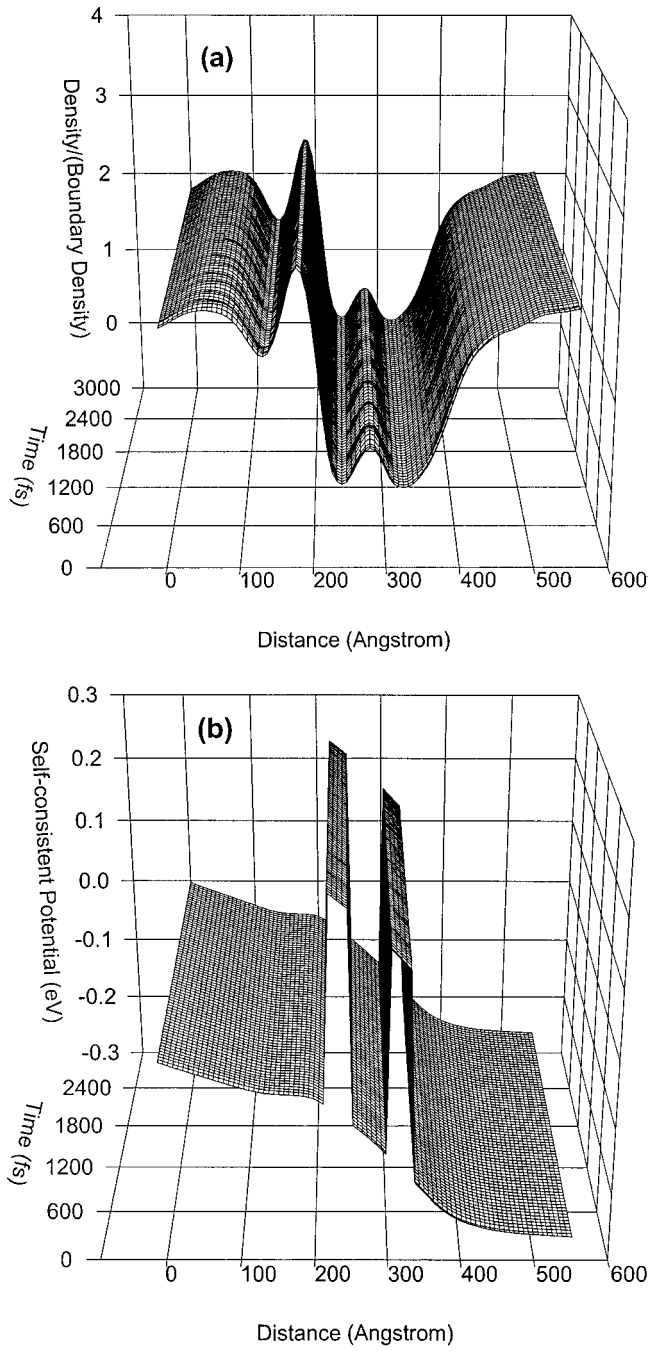

FIG. 7. Time-dependent electron density distribution, (a) self-consistent potential and (b) at bias voltage 0.264 V. The figures show that the oscillation of potential disappears. The density just oscillates a little while and then enters into a stable state. The depth of the EQW is still increasing.

Figures 11–15 show the current density, self-consistent potential, and electron density in the backward bias sweep, for which the current oscillation exists in the range of 0.240–0.256 V. The bias-voltage point where the EQW is created is smaller than the collapse bias-voltage point in the forward bias sweep. The EQW is shallower than that in the forward bias sweep. Figures 11–15 clearly show the creation and disappearance of an EQW and the density distribution.

B. Energy-level coupling model and explanation of the numerical results

The controversial issues stated above relate to the explanation of the *I-V* curve in the negative differential region. We focus our attention to this region.

The key points to explaining these issues are the creation of an EQW after the bias voltage is just greater than the resonance bias and then the coupling between the energy

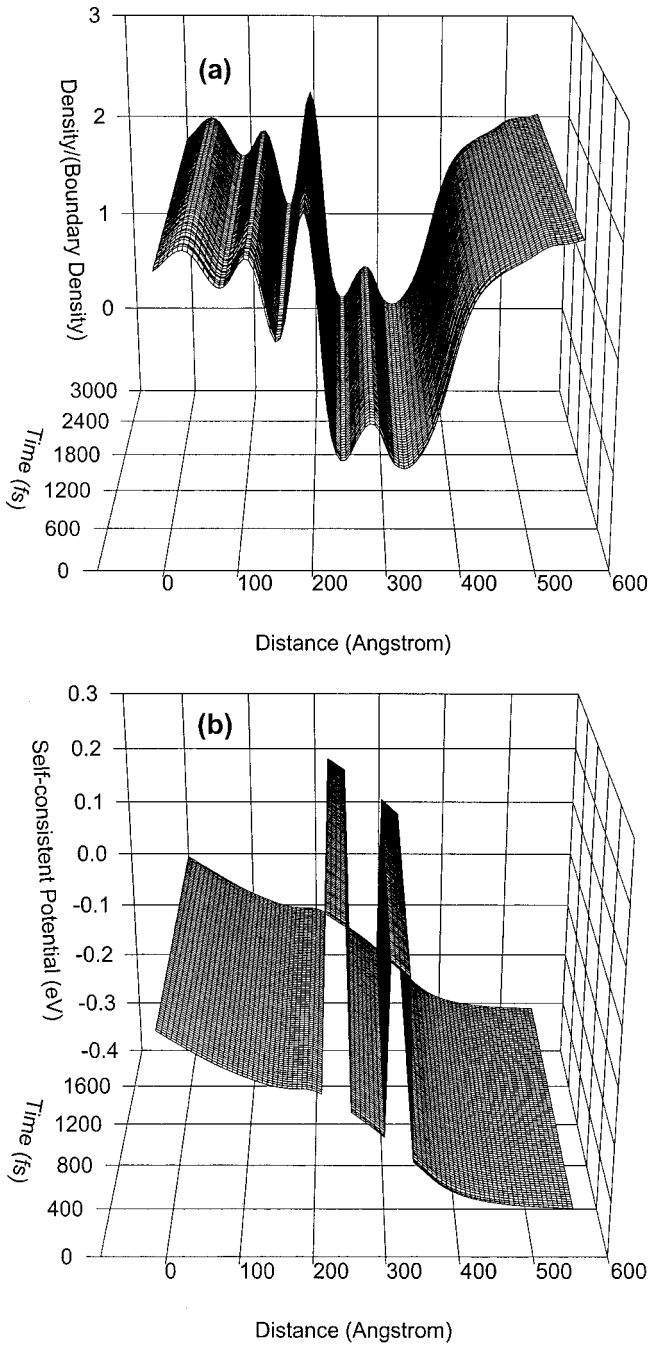

FIG. 8. Time-dependent electron density distribution, (a) self-consistent potential and (b) at bias voltage 0.312 V. The figures show that the oscillation of potential and density disappears. The depth of the EQW is the deepest. It should be noted that the density of electrons in the MQW does not change too much compared to that at bias voltage 0.232 V.

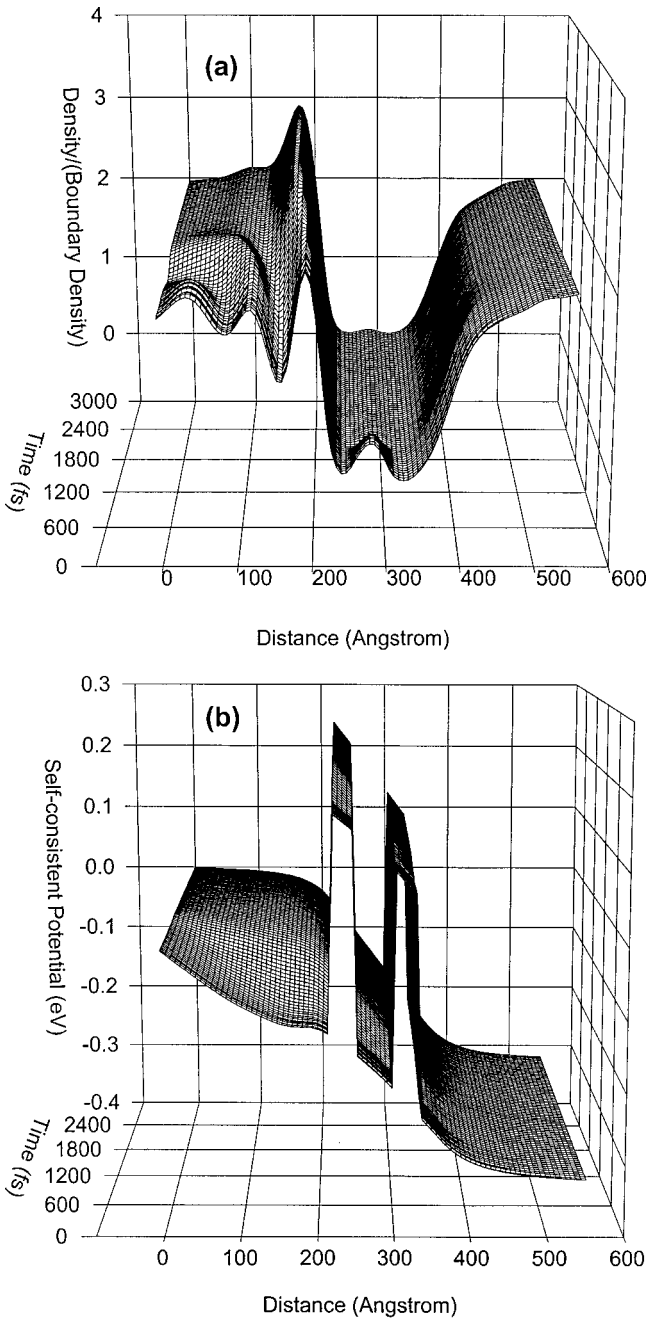

FIG. 9. Time-dependent electron density distribution, (a) self-consistent potential and (b) at bias voltage 0.320 V. These figures clearly show the collapse of the EQW and the density change while the EQW collapses. While the EQW collapses, the electron density in the main quantum well dramatically reduces to a very lower value. This leads to the transition of current from a high-current state to a lower-current state.

levels in the EQW and the MQW. As we have stated in our earlier paper,[16] after the bias voltage passes the resonance bias, the dramatic increase of the reflection coefficient of the double-barrier quantum well system leads to the dramatic increase of the amplitude of the reflected electron wave. Then, the interference between the injected and the reflected electron wave causes the depletion of the electron density in some part of the emitter. The depletion of electron in front of the emitter barrier leads to a relatively positive charge background, thereby a potential drop. An EQW is formed in this process. With the increase of the depth of the EQW with increasing bias voltage, the energy level in the EQW can obviously be distinguished from the three-dimensional states in the emitter. Thus, the interaction between the energy level in the EQW and that in the MQW will greatly influence the transport of electrons through the double-barrier quantum

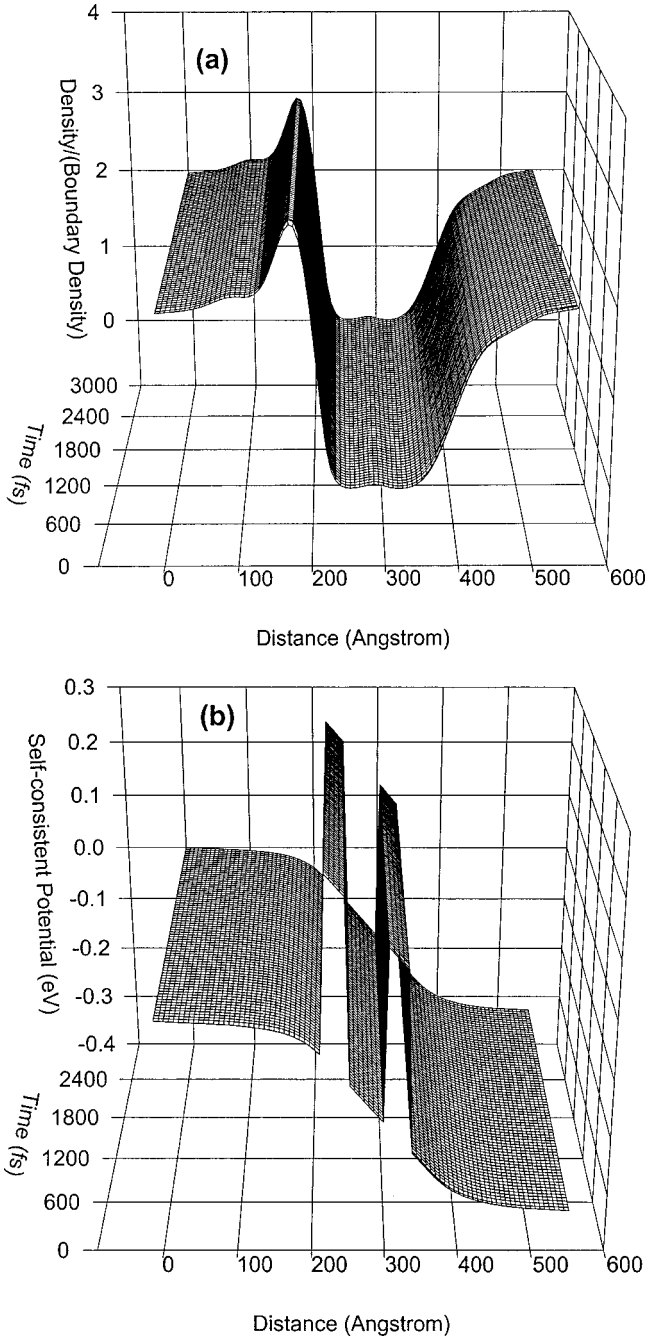

FIG. 10. Time-dependent electron density distribution, (a) self-consistent potential and (b) at bias voltage 0.328 V. The depletion of electrons in front of emitter barrier disappears. The forms of the potential and density distribution are almost the same as those at bias voltage 0.232 V except that the density of electrons in the MQW remains at a very low value.

well systems. There are several factors jointly influencing the tunneling process. The coupling between the energy level in the EQW and that in the MQW will lift the energy level in the MQW. The bias voltage applied on the structure has the tendency to push the energy in a downward direction. The strength of these two opposite factors jointly determine the average slope of the *I-V* curve. Once the influence of these two factors reaches a balanced state, a plateaulike structure

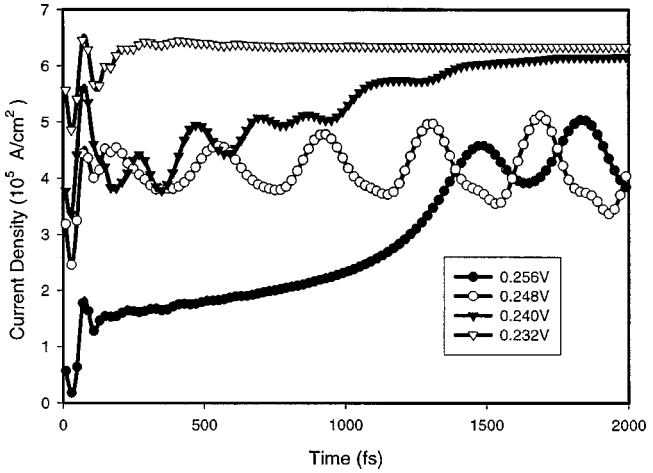

FIG. 11. Current-time characteristics of the RTD with bias voltages as parameters in the case of forward bias sweep. No current oscillations exist.

appears in the *I-V* curve. Figures 1–7 show that after the creation of the EQW, the current oscillation starts. With the increase of the bias voltage, the oscillation becomes a damped oscillation. These phenomena can also be explained by the above-stated energy-level coupling model.

Although the above statement is clearly supported by our detailed numerical simulation, it is perhaps more helpful to offer a less rigorous, yet more transparent explanation of the pivotal point of the whole argument, i.e., the coupling of the two discrete levels in the coupled emitter quantum well/main quantum well system. Suppose that the wave functions of electron in the EQW and MQW can be expressed, respectively, by

$$\psi_{\mathrm{EQW}}(z,t)=C_{\mathrm{EQW}}(z,t)e^{iE_{\mathrm{EQW}}t/\hbar}, \tag{23}$$

$$\psi_{\mathrm{MQW}}(z,t)=C_{\mathrm{MQW}}(z,t)e^{iE_{\mathrm{WQW}}t/\hbar-\gamma t}. \tag{24}$$

In writing the wave functions above, we have assumed that the width of the energy level in the MQW is much wider than that in the EQW. Considering that the energy level in the MQW is next to the three-dimensional states and the energy level in the EQW is a quasibounded state, this assumption is a very good one. The strong oscillations of density in the emitter, shown by Figs. 4(a)–6(a), support this assumption. The coupled state can be expressed by the following wave function:

$$\psi(z,t)=C_1\psi_{\mathrm{EQW}}(z,t)+C_2\psi_{\mathrm{MQW}}(z,t). \tag{25}$$

With this wave function, the current density can be expressed as

$$\begin{aligned}\langle\psi|j|\psi\rangle=&|C_1|^2\langle C_{\mathrm{EQW}}|j|C_{\mathrm{EQW}}\rangle\\&+|C_2e^{-\gamma t}|^2\langle C_{\mathrm{MQW}}|j|C_{\mathrm{MQW}}\rangle\\&+2\,\mathrm{Im}(C_1^*C_2\langle C_{\mathrm{EQW}}|j|C_{\mathrm{MQW}}\rangle e^{i(E_{\mathrm{MQW}}-E_{\mathrm{EQW}})t/\hbar-\gamma t}).\end{aligned} \tag{26}$$

The electron density can be expressed as

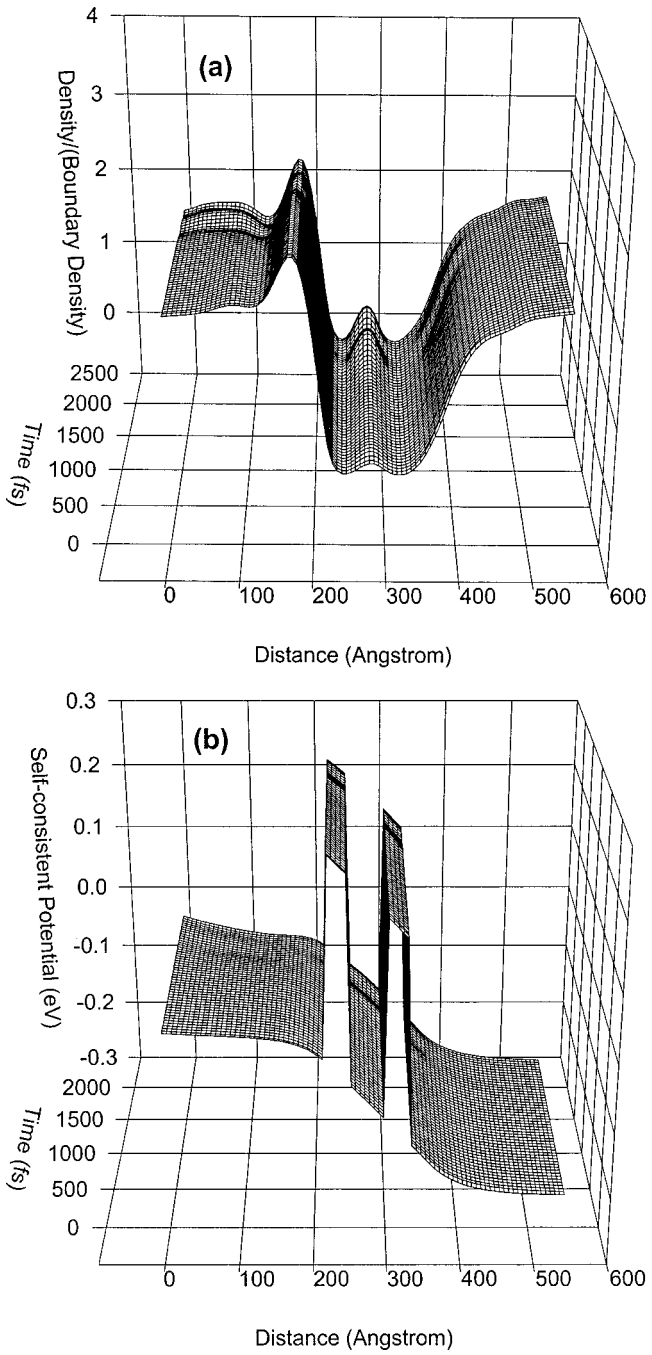

FIG. 12. Time-dependent electron density distribution, (a) self-consistent potential and (b) at bias voltage 0.256 V in backward bias sweep. From these figures we can see the oscillation creation of the density and the potential. The average density of electrons in the MQW increases with an increase of simulation time.

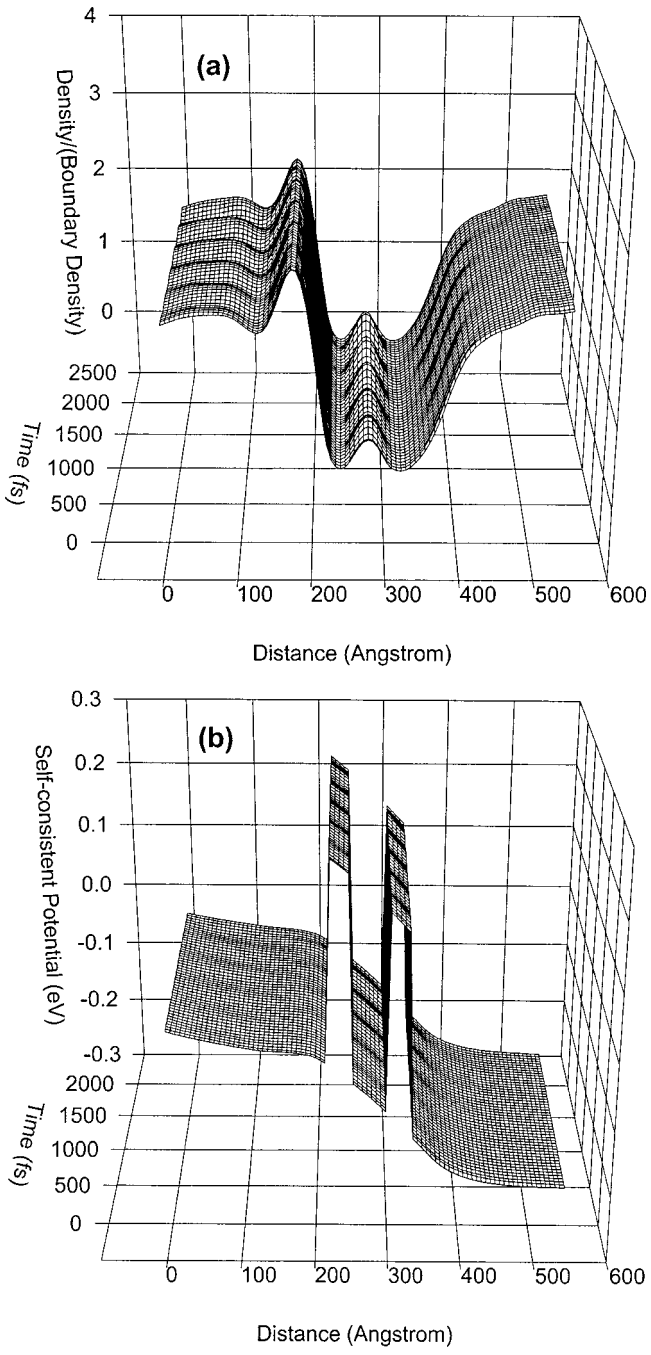

FIG. 13. Time-dependent electron density distribution, (a) self-consistent potential and (b) at bias voltage 0.248 V in backward bias sweep. These figures show the stable states of the density oscillation and potential oscillation.

$$|\psi|^2 = |C_1|^2\langle C_{\mathrm{EQW}}|C_{\mathrm{EQW}}\rangle + |C_2 e^{-\gamma t}|^2\langle C_{\mathrm{MQW}}|C_{\mathrm{MQW}}\rangle + 2\,\mathrm{Im}(C_1^* C_2\langle C_{\mathrm{EQW}}|C_{\mathrm{MQW}}\rangle e^{i(E_{\mathrm{MQW}}-E_{\mathrm{EQW}})t/\hbar-\gamma t}). \tag{27}$$

These two equations can explain the main features shown by the figures presented in this paper. As we have stated above, the time-dependent current density decays almost exponentially with time and then oscillates while the EQW is creating (for example, when the bias voltage is equal to 0.24 V). The first term in Eq. (26) sets the current value at which the oscillation is surrounded at steady states. The second term in Eq. (26) correctly reflects the damping of the curve. It should be noted that the coupling between the above-stated energy levels increases with elapsed time since the EQW is experiencing the process of creation. At that moment, the coupling, $C_1^* C_2\langle C_{\mathrm{EQW}}|j|C_{\mathrm{MQW}}\rangle$, in the third term of Eq. (26) becomes more and more important. Thus, the current oscillation appears.

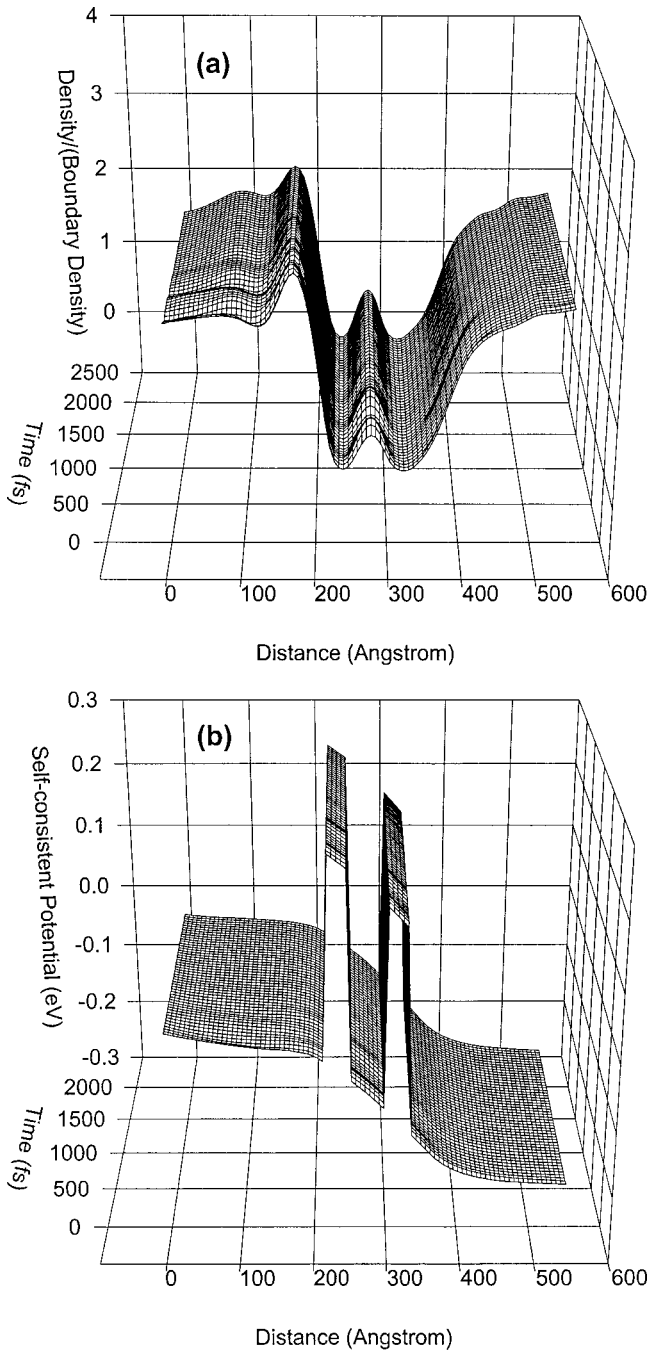

FIG. 14. Time-dependent electron density distribution, (a) self-consistent potential and (b) at bias voltage 0.240 V in backward bias sweep. These figures show the disappearance of the density oscillation and potential oscillation. The density of electrons in the MQW increases again with an increase of simulation time.

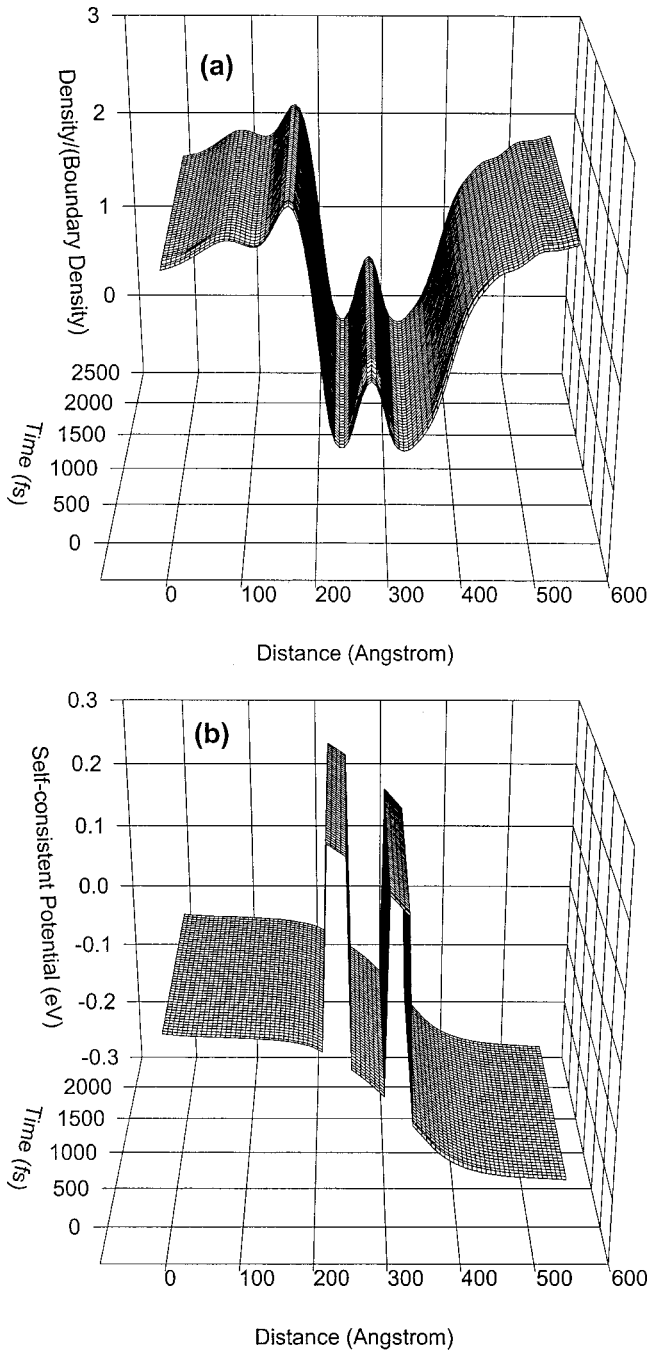

FIG. 15. Time-dependent electron density distribution, (a) self-consistent potential and (b) at bias voltage 0.232 V in backward bias sweep. The forms of the potential and density distribution are same as those in forward bias sweep at the same bias voltage.

The *I-V* curve at bias voltage 0.264 V can also be explained in the same way. The difference between these two curves is that the damping constant at bias 0.264 V is greater than that at 0.240 V since the strength of the electron-phonon interaction is stronger at higher bias voltages. It should also be noted that in the vicinity of 0.248 V, there is a bias window in which the current oscillation is almost undamped. There are two factors influencing the current oscillation. The influence of the strength of the electron-phonon interaction is to decay the oscillation. The influence of the strength of the coupling between the energy levels is to increase the amplitude of the oscillation. If the latter is greater than the former, oscillation of current develops. If these two factors reach a balanced state a BVW is created. Furthermore, if the latter is less than the former, the current experiences a damped state. In fact, with the increase of bias voltages from 0.224 to 0.312 V, the relationship between the effect of energy-level coupling and that of the electron-phonon scattering experiences the relation stated above. In the BVW, the current is

oscillating. A separate calculation shows that the energy level in the EQW is of the order of 10 meV. Thus, the oscillation frequency is the order of 1 THz,[16] as is shown in Fig. 2. Experimental results in the BVW should be the average of the oscillating current. In our model, the average of the current is expressed as

$$\langle \psi|\tilde{j}|\psi\rangle = \frac{1}{T}\Bigg[|C_1|^2\langle C_{\mathrm{EQW}}|j|C_{\mathrm{EQW}}\rangle + |C_2|^2\langle C_{\mathrm{MQW}}|j|C_{\mathrm{MQW}}\rangle \frac{1}{2\gamma}(1-e^{-2\gamma T})\Bigg] + 2\,\mathrm{Im}[C_1^* C_2\langle C_{\mathrm{EQW}}|j|C_{\mathrm{MQW}}\rangle A(T)], \quad (28)$$

where

$$A(T) = \frac{1}{T}\int_0^T dt\, e^{i(E_{\mathrm{MQW}}-E_{\mathrm{EQW}})t/\hbar - \gamma t}. \quad (29)$$

Obviously, the time average of current density is a nonzero value. It gives the values of current density in the negative differential resistance region. It is very important to note that the EQW still exists even if the current oscillation disappears. This is the foundation of our time-independent energy-level coupling model.[16] Equation (27) suitably reflects the main features of the electron density in time domain.

When the bias voltage increases to a critical value, for example, 0.320 V for the RTS employed in this paper, the positions of the above-stated energy levels are reversed. At that moment, the coupling between the energy level in the EQW and that in the MQW, and the applied bias jointly push the energy level in the MQW in a downward direction. This process sets up a milestone at which the plateaulike structure in the *I-V* curve and the EQW collapse appear (see Fig. 9). In fact, before the extinction of the EQW, there are several processes jointly determining the depth of the EQW. These processes include the electron-phonon interaction in the emitter, which dissipates electrons into the well, interference between the injected and the reflected electron waves, which depletes electrons in the emitter and leads to the formation of the EQW, and the applied bias, which drives electrons into the EQW to fill the energy level in the well. Of course, the relative position of the two energy levels is the key point in determining the existence of the EQW. The above-mentioned three factors directly determine the position of the energy level in the EQW, thereby indirectly the existence of the EQW. Once the EQW disappears, the fundamentally physical process of the tunneling is the same as that before the creation of the EQW.

In the backward bias sweep, the bias sweeps from higher to lower bias voltages. This sequence of bias sweeping causes the energy level in the MQW to be lower than the conduction-band edge of the emitter when the sweeping starts. The interaction between the energy level in the MQW and the conduction-band edge depresses the energy level in the MQW and postpones the increase of the energy level. This is the mechanism of the creation of the hysteresis of the *I-V* curves. Once the energy level in the MQW passes the conduction-band edge, the electrons accumulated in front of the emitter barrier will decrease. This and the interference between the injected and the reflected electron waves favor the creation of an EQW in a backward bias sweep. It should be noted that the depth of the EQW is much less than that in the case of the forward bias sweep [comparing Figs. 5(b) and 13(b)]. Although the creation of the EQW can influence the charge buildup in the MQW, thereby the potential and the energy level in the MQW, this influence is not big enough to cause the oscillation of current in a wider range of bias voltage. This is because the EQW is too shallow and further decreasing of the bias voltage will lead to the disappearance of the EQW as described by Fig. 14(b).

IV. ORIGIN OF HYSTERESIS AND PLATEAULIKE STRUCTURE IN *I-V* CHARACTERISTICS OF RTD

In this section, we will further analyze our theory and previous theories in resonant tunneling. Numerical simulations show that there are intrinsic current oscillations. We find that the oscillations are quickly damped and the EQW still exists when the oscillation disappears. These occurrences set up the foundation of our time-independent energy-level coupling model.[16] An important issue is the action of the charges in the MQW while the electrons flow through the double-barrier quantum well system. Previous theories realized the significance of charge buildup in the MQW. These theories predicted that there are two current states, but also the creation and the disappearance of the two states. Our theory notes the action of energy-level coupling in the process of electron transport through a double-barrier quantum well system. In fact, the influence of energy-level coupling can be seen even in the RTS's that do not exhibit a plateaulike structure in the *I-V* curve. The asymmetry of the *I-V* curve with respect to the resonance bias voltage is caused partially by the coupling between the energy level in the MQW and the three-dimensional states while the energy level in the MQW approaches the emitter Fermi energy. Once we have noted the importance of the energy-level coupling in the process of resonant tunneling, we can systematically explain the origin of hysteresis and plateaulike structure in *I-V* characteristics and the origin of the IHFCO of RTD since they are different aspects of the same problem.

After the bias voltage passes the resonance bias, the transmission coefficient of the double-barrier quantum well system decreases dramatically. This leads to the sudden increase of the reflection coefficient of the system. With an increase of the reflection coefficient, the amplitude of the reflected electron wave can be compared to the amplitude of the injected electron wave. Thus, the interference between these two kinds of electron waves leads to the depletion of electrons in front of the emitter barrier, thereby causing the relative positive charge density in the emitter and the creation of an EQW. The coupling between the energy level in the EQW and that in the MQW will cause two events. First, it leads to the IHFCO, which has been explained previously. Second, from the point of view of the time average, it raises the energy level in the MQW. Once the influence of the coupling balances that of the bias on the energy level in the MQW, a plateaulike structure in the *I-V* curve appears. Since this

kind of process can only occur after the bias passes the resonance bias, this explains that why the the plateaulike structure occurs just after the current passes its main maximum value and why the plateaulike structure in the *I-V* curve starts its formation while the charge density in the well is decreasing. From this we can predict that a plateaulike structure in the *I-V* curve can also exist after the second energy level in the MQW passes the Fermi energy level in the emitter. In our model, the extinction of the plateaulike structure is the result of the reversed position of the energy levels in the EQW and MQW. This process occurs when the energy level in the MQW passes that in the EQW. Once the energy level in the MQW is lower than that in the EQW, the quantum force created by coupling between this two energy levels will push the energy level in the MQW down, instead of raising it. Thereafter, the EQW will be filled quickly since the conducting energy level, the energy level in the MQW, is lower than that in the EQW. The tunneling through the emitter barrier into the energy level in the MQW stops. Thus, the EQW disappears. Figure 9 clearly exhibits this process. In the backward bias sweep, the system is initially in a higher bias state, and there are more electrons accumulated in front of the emitter barrier. The accumulation of electrons in front of the emitter barrier forms a screening of the applied bias, thereby reducing the influence of the bias on the energy level in the MQW. More importantly, the coupling between the MQW energy level and the conduction-band edge in the emitter depresses the MQW energy level. This mechanism postpones the rising of the current when the bias decreases. With further reduction of the bias, the amount of electrons accumulated in front of the emitter barrier decreases because of the alignment of the MQW energy level and the conduction-band edge in the emitter. At that moment, the effects of interference between the injected and the reflected electron waves feeds the accumulation of electrons in front of the emitter barrier, which leads to the formation of an EQW. The formation of the EQW leads to a situation where the QW state lies between the emitter conduction band and the EQW state. Hence, the RTS current increases rapidly to the value approximate to the plateau value. Here, the resulting ordering of the quantum states (i.e., MQW state $<$ EQW state) and the quantum interaction tends to hold the MQW state down. This physical situation tends to maintain the current density at nearly a constant value over the backward bias sweep plateau region. It should be noted that the current oscillation does not exist in the backward sweep. This is due to the EQW being too shallow to provide enough adjustment to energy level in the MQW. The current oscillation caused by coupling between energy levels is quickly damped by the electron-phonon interaction. As the bias progressively increases, the device eventually reaches another critical point. Then, the coupling between the energy level in the MQW and the three-dimensional continuum states depresses the MQW energy level, thereby postponing the increase of the current again. When the energy level in the MQW approaches the three-dimensional energy, there is a large increase in current that marks the rapid ascent to the peak *I-V* characteristic value, where the MQW energy level aligns with the energy of the three-dimensional states in the emitter.

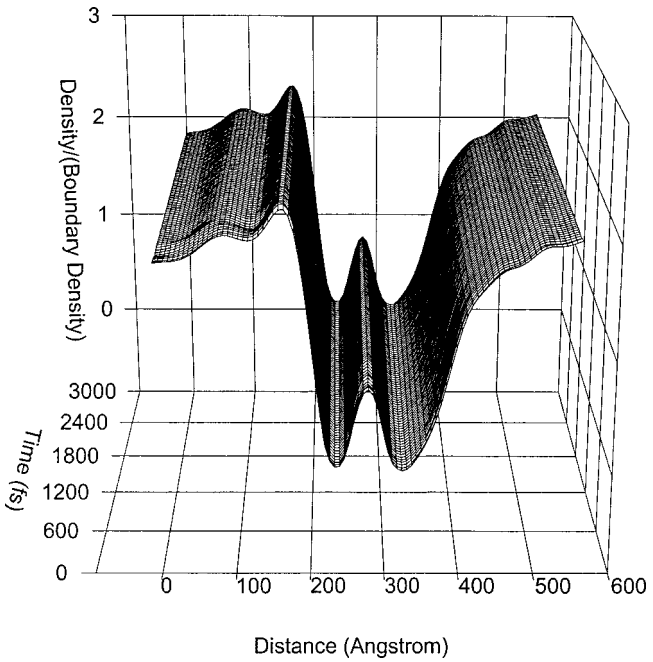

FIG. 16. Time-dependent electron density distribution at bias voltage 0.216 V in forward bias sweep.

Thus, we successfully explain the creation of the hysteresis and the feature of the *I-V* curve in the backward bias sweep.

It should be emphasized here is that the GTC theory can only explain the existence of two current states by involving charge buildup in the well-known tunneling formula. It cannot explain all the above-mentioned problems. In fact, the charge buildup is not the fundamental cause for the formation of the hysteresis of the *I-V* curves. Comparing Fig. 16 to Fig. 3, we can see that the charge trapped in the MQW at bias voltage 0.216 V is the same as that at bias voltage 0.232 V. The GTC theory cannot explain why the plateaulike structure does not develop at 0.216 V. Figures 3(a)–10(a) and Figs. 12(a)–15(a) show that the charge-buildup processes in forward bias sweep and backward bias sweep are different. Charge buildup in the MQW is not the fundamental cause influencing the formation of the *I-V* characteristics of the resonant tunneling through a double-barrier quantum well system. Furthermore, if the nonlinearlity is caused solely by charge in the MQW, we cannot explain why there is no current oscillation at bias voltage 0.216 V. Thus, charge buildup in the MQW is also not the fundamental cause of the intrinsic current oscillation.

V. CONCLUSION

By using a time-dependent finite-difference technique, we numerically solved the coupled Wigner-Poisson equations. Based on our numerical results, a time-dependent energy-level coupling model is presented to explain two long-time unsolved resonant tunneling device physical problems: the origin of hysteresis and plateaulike structure in the *I-V* curve of RTS's and the origin of the intrinsic high-frequency current oscillation in the RTS at fixed bias voltages. We believe

that these two questions are different aspects of the same problem. In our theory, the plateaulike structure in the *I-V* curve is created by the coupling between the energy levels in the EQW and MQW; the strength of the coupling determines the average slope of the plateaulike structure; the hysteresis of the *I-V* curve is the result of the coupling between the energy level in the MQW and the conduction-band edge of the emitter and the three-dimensional states in the emitter; the intrinsic high-frequency current oscillation is a reflection of the wave-corpuscle duality of electrons and the coupling between the energy level in the EQW and that in the MQW. The charge buildup in the MQW is not the fundamental cause of the hysteresis and plateaulike structure in the *I-V* curve of RTD. The time average of the oscillating current is not the cause of the creation of the plateaulike structure in the *I-V* curve since the oscillation is quickly damped in the bias-voltage region of the current plateaulike structure. The above-stated two problems have been successfully and self-consistently explained. Our theory also gives a detailed explanation on the current transition between the high-current state and lower-current state. Based upon our theory, a new bias-voltage region in which the current oscillates can be predicated.[25]

ACKNOWLEDGMENTS

The work at Stevens Institute of Technology was supported by the U.S. Office of Naval Research (Contract No. N66001-95-M-3472), and by the U.S. Army Research Office (Contracts No. DAAH04-94-G0413 and No. DAAG55-97-10355).

[1] L. L. Chang, L. Esaki, and R. Tsu, Appl. Phys. Lett. **24**, 593 (1974).
[2] V. J. Goldman, D. C. Tsui, and J. E. Cunningham, Phys. Rev. Lett. **58**, 1256 (1987).
[3] W. R. Frensley, Phys. Rev. Lett. **57**, 2853 (1986).
[4] K. L. Jensen and F. A. Buot, Phys. Rev. Lett. **66**, 1078 (1991).
[5] B. A. Biegel and James D. Plummer, Phys. Rev. B **54**, 8070 (1996).
[6] N. C. Kluksdahl, A. M. Kriman, D. K. Ferry, and C. Ringhofer, Phys. Rev. B **39**, 7720 (1988).
[7] M. V. Fischetti, J. Appl. Phys. **83**, 270 (1998).
[8] G. Klimeck, T. B. Boykin, R. C. Bowen, and R. Lake, in 5th Annual Device Research Conference Digest, IEEE Press, 1997.
[9] W. R. Frenslay, Rev. Mod. Phys. **62**, 745 (1990).
[10] W. Pötz, Phys. Rev. B **41**, 12 111 (1990); J. Zhang and W. Pötz, Phys. Rev. B **42**, 11 366 (1990); M. A. Talebian and W. Pötz, Superlattices Microstruct. **20**, 267 (1996).
[11] T. C. L. G. Sollner, Phys. Rev. Lett. **59**, 1622 (1987).
[12] D. L. Woolard, F. A. Buot, D. L. Rhodes, X. L. Lu, R. A. Lux, and B. S. Perlman, J. Appl. Phys. **79**, 1515 (1996).
[13] Y. Fu and M. Willamder, J. Appl. Phys. **72**, 3593 (1992).
[14] H. C. Liu, Appl. Phys. Lett. **53(6)**, 485 (1988).
[15] B. A. Biegel, Ph.D. thesis, University of California, Los Angles, (1997).
[16] Peiji Zhao, K. L. Cui, D. Woolard, K. Jensen, and F. Buot, J. Appl. Phys. **87**, 1337 (2000).
[17] Peiji Zhao, K. L. Cui, and D. Woolard (unpublished).
[18] Historically, Kluksdahl *et al.* first found the creation of an emitter quantum well (Ref. 6). Unfortunately, they were not sure of the result (Ref. 7). Thus, they did not realize the importance of the emitter quantum well. Fischetti (Ref. 7) and Biegel and Plummer (Ref. 15) also found the existence of an emitter quantum well. However, they either give a wrong explanation of the emitter quantum well (Ref. 7) or said nothing about the creation of the emitter quantum well (Ref. 15).
[19] B. Ricco and M. Ya. Azbel, Phys. Rev. B **29**, 1970 (1984).
[20] C. Presilla, G. Jona-Lasinio, and F. Capasso, Phys. Rev. B **34**, 5200 (1991).
[21] E. Wigner, Phys. Rev. **40**, 749 (1932); D. K. Ferry and H. L. Grubin, Solid State Phys. **49**, 283 (1995).
[22] F. A. Buot and K. L. Jensen, Phys. Rev. B **42**, 9429 (1990).
[23] Peiji Zhao, Norman Horing, and H. L. Cui, Philos. Mag. **80**, 1359 (2000).
[24] P. Bordone, M. Pascoli, R. Brunetti, A. Bertoni, and C. Jacoboni, Phys. Rev. B **59**, 3060 (1999).
[25] Peiji Zhao, H. L. Cui, and D. Woolard (unpublished).